We are IntechOpen, the world's leading publisher of Open Access books
Built by scientists, for scientists

6,900
Open access books available

186,000
International authors and editors

200M
Downloads

Our authors are among the

154
Countries delivered to

TOP 1%
most cited scientists

12.2%
Contributors from top 500 universities

CLARIVATE ANALYTICS
BOOK CITATION INDEX
INDEXED

WEB OF SCIENCE™

Selection of our books indexed in the Book Citation Index
in Web of Science™ Core Collection (BKCI)

Interested in publishing with us?
Contact book.department@intechopen.com

Numbers displayed above are based on latest data collected.
For more information visit www.intechopen.com

Dual Active Contour Models for Medical Image Segmentation

Gilson Giraldi[1], Paulo Rodrigues[2], Jasjit Suri[3,4] and Sameer Singh[5]

[1]National Laboratory for Scientific Computing (LNCC)
[2]FEI University
[3]Biomedical Technologies, Inc. Denver,
[4]Idaho State University,
[5]Loughborough University,
[1,2]Brazil
[3,4]USA
[5]UK

1. Introduction

Deformable Models, which includes the popular snake models (Kass et al., 1988) and deformable surfaces (McInerney & Terzopoulos, 1996; Suri & Editors, 2006), are well known techniques for boundary extraction and tracking in 2D/3D images. Basically, these models can be classified into three categories: parametric, geodesic snakes and implicit models. The relationships between these models have been demonstrated in several works in the literature (Sapiro, 1997).

Parametric Deformable Models consist of a curve (or surface) which can dynamically conform to object shapes in response to internal (elastic) forces and external forces (image and constraint ones) (Suri & Editors, 2006). Snake models, also called active contour models, are *2D* deformable models proposed by Kass at al. (Kass et al., 1988) which have been successfully applied in a variety of problems in computer vision and image analysis. Its mathematical formulation makes easier to integrate image data, an initial estimated, desired contour properties and knowledge-based constraints, in a single extraction process (Suri & Editors, 2006).

In fact, despite of the mentioned capabilities, parametric models in general can not deal with topological changes. Among the approaches to deal with the topological limitations of the traditional snake model (Bischoff & Kobbeit, 2004; Oliveira et al., 2004), the T-Snakes has the advantage of being a general one (McInerney & Terzopoulos, 1999). Besides, parametric models are too sensitive to their initial conditions due to nonconvexity problems (see (Davatzikos & Prince, 1999) and references therein). To address this limitation some authors have proposed multiscale techniques (Leymarie & Levine, 1993), dynamic program (DP) (Amini et al., 1990)and dual methods, also called dual snakes (Gunn & Nixon, 1997). The non-invariance under affine transformations is another limitation of the traditional snake models. As a consequence, the internal energy is sensitive to distortions due to changes in viewing geometry. From a dynamical point of view, it means that the elastic forces may

affect the efficiency of the energy minimization process (Ip & Shen, 1998). Some methods have been proposed to address this problem (Giraldi & Oliveira, 2004; Ip & Shen, 1998), even in the context of dual active contour models (Gunn & Nixon, 1997).

The basic idea of the dual snakes is to reject local minima by using two contours: one which contracts from outside the target and one which expands from inside. Such proposal makes possible to reduce the sensitivity to initialization through the comparison between the two contours energy and positions. The two contours are interlinked to provide a driving force to carry the contours out of local minima, which makes the solution less sensitive to the initial position (Gunn & Nixon, 1997).

In (Giraldi et al., 2000b), it is presented an extension of the dual method through the T-Snakes. The dual approach was embedded in the T-Snakes framework to propose a generalized dual method: one T-snake contracts and splits from outside the target(s) and the other one(s) expand(s) from inside in the process of seeking for the objects boundaries in an image. Such generalization, called the Dual-T-Snakes model, allows to address some limitations of the dual approach proposed in (Gunn & Nixon, 1997) and offers an efficient framework for dual surface models.

In (Suri & Editors, 2006) some of us present an implicit formulation for dual snakes, based on the level set approach. The key idea of that work is to view the inner/outer contours as a level set of a suitable embedding function. The mathematical background of the method is explained and its utility for segmentation of cell images discussed. Besides, a fast dual front implementation of active contours has been proposed in (Li & Yezzi, 2005) and applied for segmentation of $2D$ images. The method is motivated by minimal path technique (Cohen, 2001; Cohen & Kimmel, 1996) and uses fast marching methods (Sethian, 1999) to compute the minimal partition curve that represents the object boundary. The same formulation can be used for both $2D$ and $3D$ and it was applied for segmentation of the brain cortex (Li & Yezzi, 2005).

Dual active contour models have been applied for feature and geometric measures extraction (Gunn, 1996), boundary extraction on ultrasound images (Chen et al., 2001; 2002), brain surface extraction from PET images (Tohka et al., 2004) and cell image segmentation based on a two stage approach (Bamford & Lovell, 1997; Giraldi et al., 2000b) : (1) the region of interest is reduced; (2) a search based technique, like dynamic programming, is used to find the object boundaries.

In this chapter we review parametric and implicit dual snake models. Following, in section 2, we offer some background for the material. Section 3 gives a review of parametric dual models. The Dual-T-Snakes algorithm and the cell-based dual snake model are discussed in this section. Following, in section 4 we describe the implicit formulations for dual snakes: the Dual-Level-Set and Dual-Front methods. During the presentation of these methods, we show results in medical image segmentation. We offer a discussion on section 5 by comparing the presented methods and by pointing out drawbacks of dual approaches. In section 6 we present the conclusions and future developments in dual approaches.

2. Background review

The original snake model (Kass et al., 1988) is formulated as a functional energy minimization process that consists of an initial model which is carried to the desired object boundary by forces described by the Euler-Lagrange equations. In a different way, the snake evolution can be formulated by local deformations to dynamically reshape the initial model

in a process which do not apply minimization techniques explicitly. This approach is used in the T-Snakes model which is revised in section 2.1. On the other hand, implicit formulations based on the level set method can be used, as we shall see in section 2.2.

2.1 T-Snakes model

The classical snake model proposed in (Kass et al., 1988) do not incorporate topological changes. Among the proposals for incorporating topological capabilities to parametric snake models (Bischoff & Kobbeit, 2004; Oliveira et al., 2004), the T-Snakes approach (McInerney & Terzopoulos, 1999) has the advantage of been a general one, in the sense that the same formulation can be used for 2D and 3D, for both splits and merges.

The T-Snakes approach is composed basically by four components (McInerney & Terzopoulos, 1999): (1) a simple CF-triangulation of the image domain; (2) projection of each snake over the grid; (3) a binary function called characteristic function χ, defined on the grid nodes, which distinguishes the interior from the exterior of a snake; (4) a discrete snake model.

To clear the ideas, consider the characteristic functions (χ_1 and χ_2) relative to the two contours pictured in Figure 1. The vertices marked are those where $\max\{\chi_1, \chi_2\} = 1$. Observe that the merge of the curves belongs to the triangles in which the characteristic function changes value.
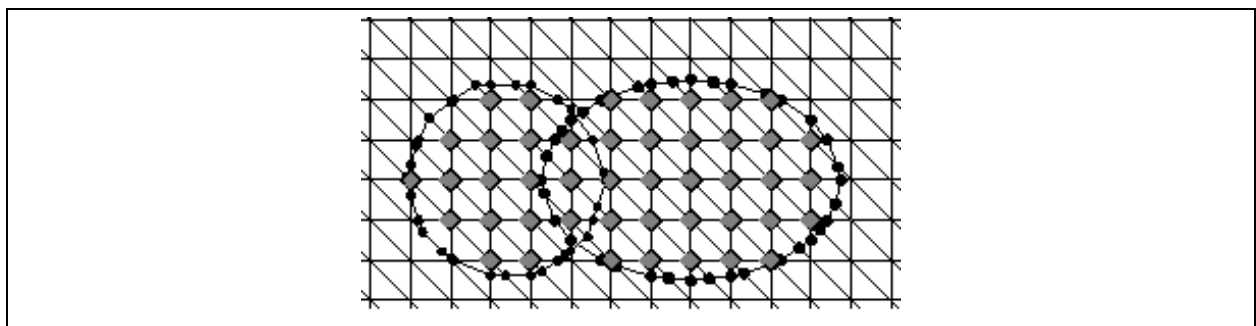

Fig. 1. Two snakes colliding with the inside grid nodes and snake points (snaxels) marked.

Thus, from the points obtained in the step (2), we can choose a set of N points $\{v_i = (x_i, y_i), i = 0, ..., N-1\}$ to be connected to form a closed contour (T-Snake). In (Giraldi et al., 2003)we evolve a T-Snake based on a tensile force (B_i), an external (image) force (f_i), and a normal (balloon-like) force (F_i), defined as follows:

$$B_i = w_1 \left(\frac{v_{i-1}^t - 2v_i^t + v_{i+1}^t}{(\Delta s_i)^2} \right), \tag{1}$$

$$f_i = \gamma \nabla P(v_i), \tag{2}$$

$$F_i = k(sign_i)\vec{n}_i, \tag{3}$$

where $\vec{n}_i$ is the normal at the snaxel v_i and w_1, γ, k are force scale factors, $sign_i = 1$ if $I(v_i) \geq T$ and $sign_i = 0$ otherwise (T is a threshold for the image I) and $P = -\|\nabla I\|^2$. The

utility of the balloon-like force given by expression (3) is two-fold. Firstly, it avoids the unwanted contraction effect of the tensile force due to the inflation (see
(Cohen, 1991) for details). Secondly, this force pushes the model towards the object(s) of interest, characterized by the threshold T. The external force f_i given by expression (2) attracts the snake to object boundaries in the image. We update the T-Snake position according to the evolution equation:

$$v_i^{(t+\Delta t)} = v_i^t + \Delta t \left(B_i^t + F_i^t + f_i^t \right), \tag{4}$$

where Δt is a time step. The T-Snakes model incorporates also an entropy condition: "once a node is burnt (passed over by the snake) it stays burnt " (McInerney & Terzopoulos, 1999). A specific termination condition is defined based on the number of deformations steps (temperature) that a triangle was cut by a T-Snake. A T-Snake is considered to have reached its equilibrium state when the temperature of all the snaxels fall bellow a preset value (called "freezing point" in the T-Snakes literature (McInerney & Terzopoulos, 1999)).

2.2 Level set
In this section we review some details of the level set formulation (Malladi et al., 1995). The main idea of this method is to represent the deformable surface (or curve) as a level set $\left\{ x \in \Re^3 \middle| G(x) = 0 \right\}$ of an embedding function:

$$G : \Re^3 \times \Re^+ \to \Re, \tag{5}$$

such that the deformable surface (also called front in this formulation), at *t=0*, is given by a surface S:

$$S(t=0) = \left\{ x \in \Re^3 \middle| G(x, t=0) = 0 \right\}, \tag{6}$$

The next step is to find an Eulerian formulation for the front evolution. Following Sethian (Malladi et al., 1995), let us suppose that the front evolves in the normal direction with velocity $\vec{F}$ that may be a function of the curvature, normal direction, etc.
We need an equation for the evolution of $G(x,t)$, considering that the surface S is the level set given by:

$$S(t) = \left\{ x \in \Re^3 \middle| G(x, t) = 0 \right\}, \tag{7}$$

Let us take a point $x(t)$, $t \in \Re^+$ of the propagating front S. From its implicit definition given above we have:

$$G(x(t), t) = 0, \tag{8}$$

Now, we can use the Chain Rule to compute the time derivative of this expression:

$$G_t + F |\nabla G| = 0, \tag{9}$$

where $F = \|dx/dt\|$ is called the speed function and ∇ is the gradient operator, with respect to x. An initial condition $G(x, t = 0)$ is required. A straightforward technique to define this function is to compute a signed-distance function as follows:

$$G(x, t = 0) = \pm d, \tag{10}$$

where d is the distance from x to the surface $S(t = 0)$ and the sign indicates if the point is interior (-) or exterior (+) to the initial front. The "fast marching method" (FMM) can be used to efficiently compute this function (Sethian, 1996).

Finite difference schemes, based on an uniform grid, can be used to solve equation (9). The same entropy condition of T-Surfaces (once a grid node is burnt it stays burnt) is incorporated in order to drive the model to the desired solution (in fact, T-Surfaces was inspired on the level set model (McInerney & Terzopoulos, 1999)).

In this higher dimensional formulation, topological changes can be efficiently implemented. Numerical schemes are stable, and the model is general in the sense that the same formulation holds for 2D and 3D, as well as for merge and splits. Besides, the surface geometry is easily computed. For example, the front normal ($\vec{n}$) and curvature (K) are given, respectively, by:

$$\vec{n} = \nabla G(x, t), \qquad K = \nabla \cdot \left(\frac{\nabla G(x, t)}{\|\nabla G(x, t)\|} \right), \tag{11}$$

where the gradient (∇) and the divergent ($\nabla.$) are computed with respect to x.

The update of the embedding function through expression (9) can be made cheaper if the narrow-band technique is applied. The key idea of this method comes from the observation that the front can be moved by updating the level set function at a small set of points in the neighbourhood of the zero set instead of updating it at all the points on the domain (see (Malladi et al., 1995; Sethian, 1996) for details).

3. Parametric dual models

Parametric dual active contour models have been applied for cell image segmentation (Chen et al., 2002; 2001; Giraldi et al., 2003), features and geometric measures extraction (Gunn, 1996; Gunn & Nixon, 1997). The main advantage of these methods against usual snake models is their capability to reject local minima by using two contours: one which contracts from outside the target and one which expands from inside. Such proposal makes possible to reduce the sensitivity to initialization, by enabling a comparison between the two contours energy, which is used to reject local minima. In what follows, we firstly present the original dual snake model, proposed by Gunn and Nixon (Gunn, 1996; Gunn & Nixon, 1997). Next, we review more recent approaches that incorporate topological abilities (the Dual-T-Snakes) and improve the efficiency for ultrasound images (Dual-Cell)

3.1 Original dual model

The dual snake methodology was firstly proposed in (Gunn & Nixon, 1997). To obtain the conventional continuity and smoothness constraints, but removes the unwanted contraction force, a scale invariant internal energy function (shape model) is developed. In (Gunn &

Nixon, 1997) a snake is considered as a particle system $\{v_i = (x_i, y_i), i = 0,...,N-1\}$ whose particles are linked by internal constraints. The shape model is accomplished by the following internal energy:

$$E_R = \frac{1}{N} \sum_{i=0}^{N-1} E_{\text{int}}(v_i); \qquad E_{\text{int}} = \frac{1}{2}\left(\frac{\|e_i\|^2}{h}\right), \tag{12}$$

where:

$$e_i = \frac{1}{2}(v_{i-1} + v_{i+1}) - v_i + \frac{1}{2}\theta_i R(v_{i-1} + v_{i+1}), \tag{13}$$

h is the average space step, R is a 90° rotation matrix and θ_i is related to the internal angle ϕ_i in the vertex v_i by:

$$\theta_i = \cot\left(\frac{\varphi_i}{2}\right). \tag{14}$$

The Figure 2 helps to understand the geometric meaning of these elements. In this figure, the vector e_i is such that the triangle with vertices $v_{i+1}, v_i + e_i, v_{i-1}$ is isosceles.
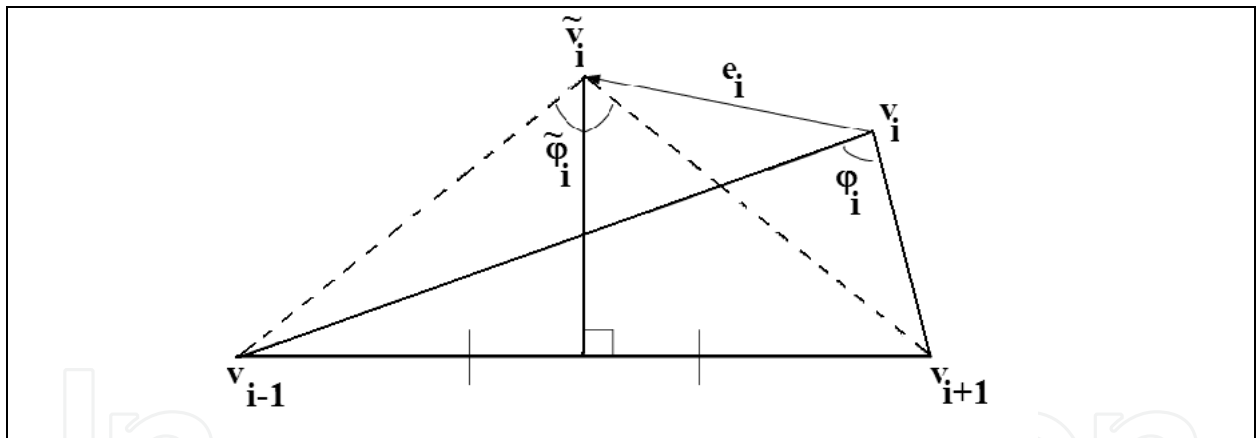

Fig. 2. Geometric elements of the local shape model. Reprinted from (Gunn & Nixon, 1997)

It is clear that E_R has a global minimum when $e_i = 0$, $i = 0,1,2,...,N-1$. From (13)-(14) it can be shown that this happens when:

$$\varphi_i = \pi(N-2)/(2N), \quad i = 0,1,...,N-1,$$

which are the internal angles of a regular polygon with vertices given by the points v_i (Gunn & Nixon, 1997). The energy (12) can be also shown to be rotation, translation and scale invariant (Gunn & Nixon, 1997). Therefore there is no tendency to contraction as already pointed out for the original snake model (see (Cohen, 1991) for details). With the internal energy given by expression (12), the curve is biased towards a regular polygon (Gunn & Nixon, 1997). As before, the external energy is defined by:

$$E_{ext}(v_i) = -\left\|\nabla I(v_i)\right\|^2.$$ (16)

The total energy of the model is given by:

$$E = \frac{1}{N}\sum_{i=0}^{N-1}\left(\lambda E_{int}(v_i) + (1-\lambda)E_{ext}(v_i)\right).$$ (17)

where λ is a smoothing parameter which lies between 0 and 1 (Gunn & Nixon, 1997). This expression guarantees that during the optimization process, the snake will seek for strong object boundaries, due to E_{ext}, whose shape resembles a regular polygon, due to shape model given by expression (12). This fact makes easier to establish the correspondence (matching) between the points of the two contours because the form of the snake during the evolution is limited by the energy (12). The methodology takes advantage of this correspondence by proposing the driving force:

$$F_{driving} = g(t)\frac{u_i - v_i^t}{\left\|u_i - v_i^t\right\|},$$ (18)

where v_i^t is the contour being processed at time t, u_i^t is the contour remaining at rest and $g(t)$ is the strength of the force. The termination condition adopted in (Gunn & Nixon, 1997) is the following one, based on low velocity criterion:

$$\max_i\left\|v_i^{t+1} - v_i^t\right\| < \delta,$$ (19)

where δ is a termination parameter.

The dual approach consists in making the inner and outer contours evolve according the following algorithm: The contour with the highest energy is selected. If its motion remains below some termination condition then the driving force (18) is increased until it moves at a rate greater than the chosen threshold δ. When the energy begins to decrease, the added driving force is removed and the contour is allowed to come into equilibrium. The procedure is then repeated until both contours have found the same equilibrium position.

3.2 Dual-T-Snakes algorithm

The key idea behind this method is to explore the T-Snakes framework to propose a generalized dual active contour model: one T-Snake contracts and splits from outside the targets and another one expand from inside the targets (Giraldi et al., 2003; 2000b).

To make the outer snake to contract and the inner ones to expand we assign an inward normal force to the first and an outward normal force to the others according to expressions (3). Also, to turn the T-Snakes evolution interdependent we use the image energy and an affinity restriction.

We use two different definitions for image energy: one for the outer contour (E_{outer}) and another one for the set of inner contours enclosed by it (E_{inner}):

$$E_{outer} = \sum_{i=0}^{N-1}\left(-\left\|\nabla I(v_i)\right\|^2\right)/N.$$ (20)

$$E_{inner} = \frac{1}{m}\left(\sum_{k=0}^{m-1}\left(\sum_{i=0}^{N_k-1}\left(-\left\|\nabla I\left(v_i\right)\right\|^2 \right) / N_k \right) \right). \tag{21}$$

where m is the number of inner curves, N, N_k are the number of snaxels of the outer snake and of the inner snake k, respectively. The normalization is necessary in order to be compared. Otherwise, the snake energy would be a decreasing function of the number of snaxels and comparisons would not make sense.

Following the dual approach methodology (Gunn & Nixon, 1997), if $E_{inner} > E_{outer}$ an inner curve must be chosen. To accomplish this, we use an affinity operator which estimates the pixels of the image most likely to lie on the boundaries of the objects. Based on this operator, we can assign to a snaxel the likelihood that it is close to a boundary. That likelihood is thresholded to obtain an affinity function that assigns to the snaxel a 0-1 value: "0" for the snaxels most likely to lie away from the target boundaries and "1" otherwise.

Then, the inner curve with highest number of snaxels with affinity function value null is chosen. If $E_{inner} < E_{outer}$ the outer snake is evolved if the corresponding affinity function has null entries.

Also, the balance between the energy/affinity of the outer and inner snakes allows to avoid local minima. For instance, if a T-Snake has been frozen, we can increase the normal force at the snaxels where the affinity function is zero, that is, we add a driving force only to the snaxels most like to lie far from the boundary. The self-intersections that may happen during the evolution of a snake when increasing the normal force are naturally resolved by the T-Snakes model. This is way we can use that added normal force to play the role of the driving force used by Gunn and Nixon (avoiding the matching problem required in (Gunn & Nixon, 1997)).

To evaluate similarity between two contours, we use the difference between the characteristic function of the outer snake and the characteristic functions of the inner ones ($Characteristic\_Diff$). For example, in the case of the CF triangulation of the Figure 1 we can stop the motion of all snaxels of an inner snake inside a triangle σ if any of its vertex $v \in \sigma$ has the two following properties: (a). All the six triangles adjacent to v have a vertex where $Characteristic\_Diff = 0$; (b). One of these triangles is crossed by the outer contour

The freezing point (section 2.1) is used to indicate that a T-Snake has found an equilibrium position. In what follows, we call Dual Snake a list of T-Snakes where the first one is an outer contour and the other ones are inner contours. The algorithm can be summarized as follows:

Algorithm 1: Dual-T-Snakes
        Put all the dual snakes into a queue.
       repeat
         Pop out a dual snake from the queue;
         Use the energies (equations (20) and (21)) and the affinity function to decide the
         snake to be processed;
       if all snaxels of that snake are frozen
         repeat
           increase the normal force at those with affinity zero
         until the snake energy starts decreasing

Remove that added normal force;
  repeat
    Evolve the snake
  until the temperature of all snaxels falls bellow the freezing point; }
    Analyze the Characteristic_Diff of the current snake;
  if the snake being processed is close to a snake of the other type (inner/outer)
    then remove the dual snake from the queue.}
  else
    mount the resulting dual snake(s) and go to the beginning.
until the queue is empty

The experience with this method shows that it is very useful to reduce the search space. So, we proposed in (Giraldi et al., 2000b) a two stage segmentation approach: (1) the region of interest is reduced by the Dual-T-Snakes; (2) a global minimization technique is used to find the object boundaries. In (Giraldi et al., 2000b) we apply the Viterbi algorithm, which is a dynamic program technique. The search space is constructed by discretizing each curve in N points and establishing a matching between them. Each pair of points is then connected by a segment which is subdivided in M points. This process provides a discrete search space, with NM points, that is pictured in the Figure 3:
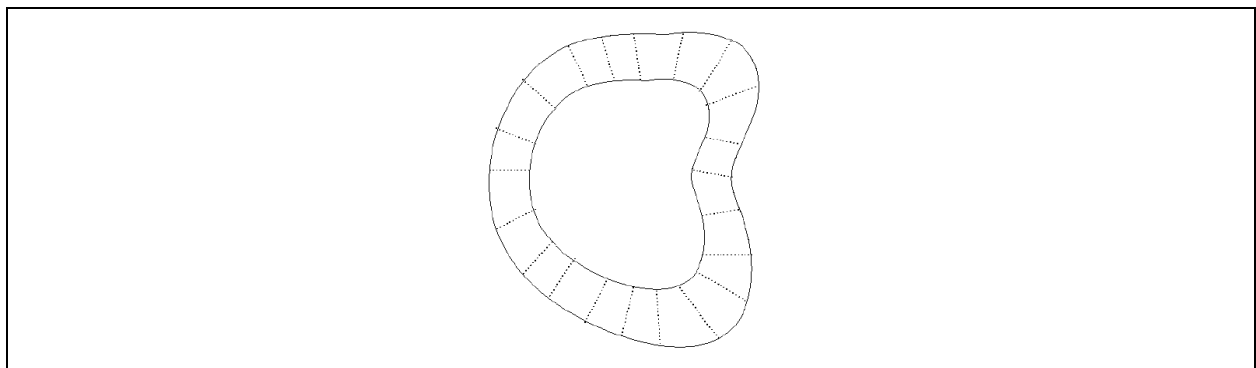

Fig. 3. Search space obtained through a matching between inner and outer snakes.

The target boundary is then determined by minimizing the following energy functional (Gunn, 1996):

$$E_{snake} = \sum_{i=0}^{N-1} E_i.$$ (22)

$$E_i = \alpha E_{\text{int}}\left(v_{i-1}, v_i, v_{i+1}\right) + \beta E_{ext}\left(v_i\right) + \lambda E_{line}\left(v_i\right).$$ (23)

with E_{int}, E_{ext} and E_{line} defined as follows:

$$E_{\text{int}}\left(v_{i-1}, v_i, v_{i+1}\right) = \left(\frac{v_{i-1} - 2v_i + v_{i+1}}{\left\|v_{i-1} - v_{i+1}\right\|}\right)^2.$$ (24)

$$E_{ext}\left(v_i\right) = -\left\|\nabla I\left(v_i\right)\right\|, \qquad E_{line} = \pm I\left(v_i\right),$$ (25)

where the real parameters α, β and λ must be chosen in advance. The Viterbi algorithm was also used in (Bamford & Lovell, 1997) and sometimes it is called non-evolutionary dual model, in the sense that it is not based on a curve evolution.

The following example shows the application of the segmentation framework that combines the Dual-T-Snakes and the Viterbi algorithm (Giraldi et al., 2000b; 2003) for a cell image. The Figure 4.a shows a blood cell obtained by an electronic microscope technique. When pass-band filter is applied, we get an edge map resembling a ribbon whose thickness depends on the kernel size of the used filter (Figure 4.b). That is an ideal situation for applying Dual-T-Snakes plus Viterbi because, firstly, the former extracts the ribbon (Figure 4.c). Then, the later is applied to the original image to give the final result (Figure 4.d).
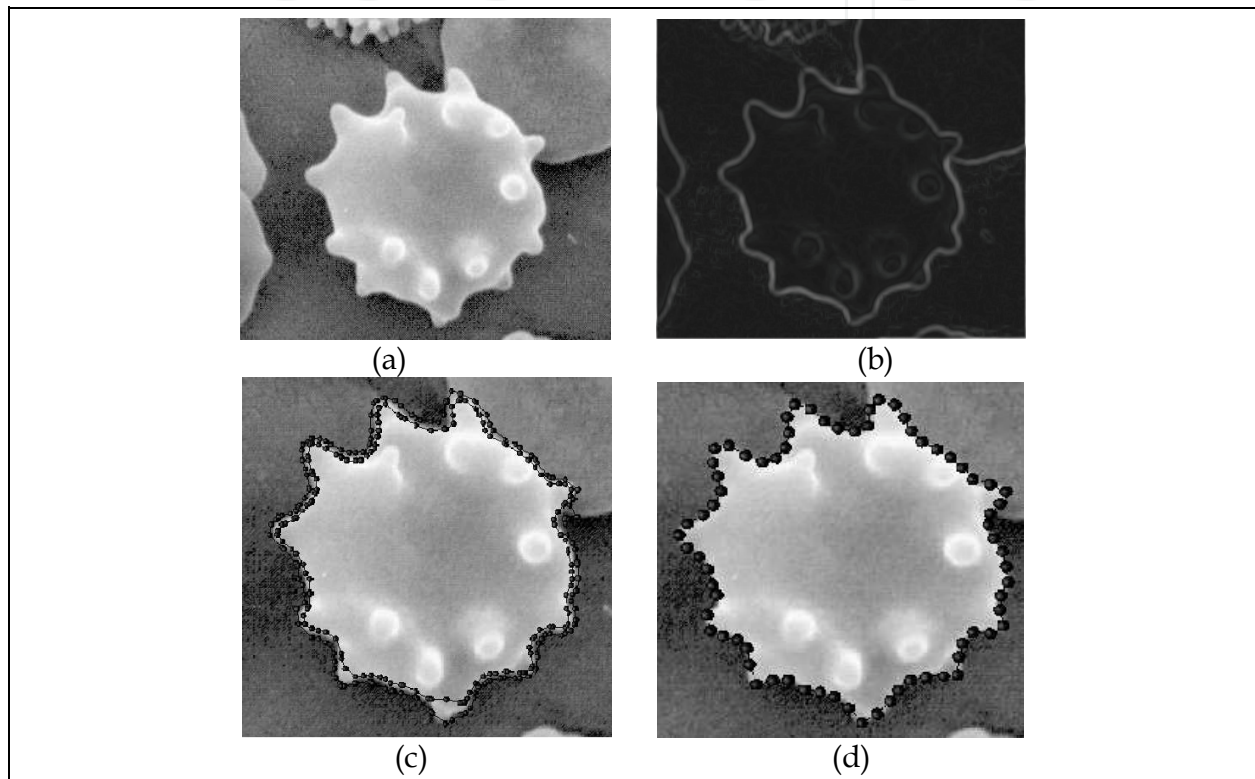
Fig. 4. Search space obtained through a matching between inner and outer snakes. (a)Image to be processed. (b)Band-Pass filtered image. (c)Dual-T-Snakes solution. (d)Viterbi solution.

3.3 Cell-Based dual snake model

In (Chen et al., 2002) it is proposed a cell-based dual snake model for ultrasound image. Boundary extraction and segmentation for this kind of image are a much harder problem than for other image modalities, due to the speckle, the tissue-related textures, and the artifacts resulting from the ultrasonic imaging process. To address such difficulties it is proposed in (Chen et al., 2002) a model which is devised into three main stages, namely, cell generation, cell-based deformation and contour smoothing. In the cell-generation stage, the immersion watershed algorithm (Vincent & Soille, 1991) is used to generate the nonoverlapped cells. To alleviate the interference of speckle in cell generation, the speckle is reduced by using the multiscale Gaussian filters before computing the gradient map. The cell boundaries are defined as the watersheds formed in the gradient map of the speckle-reduced ultrasound images.

Once the cell decomposition of the image domain is performed, we must define the dual snakes and the evolution model. Thus, given an initial contour enclosing the region of interest (ROI), a set of minimum covering cells, $C_1, C_2, ..., C_N$ containing the ROI is found, based on the cells generated in the previous stage (Figure 5). Let Γ_0 and Γ_i be the initial outer and inner snakes, respectively, which are pictured on Figure 5. The outer snake is defined as the outermost boundary of $\bigcup_{i=1}^{N} C_i$. Suppose that the center of the ROI is the cell C_1. Then, its boundary is the initial inner snake Γ_i, also represented on Figure 5.

Let Γ_1^t and Γ_2^t be the inner and outer snakes, respectively, at the deformation step t. Then, the model energy $E\left(\Gamma_1^t \cup \Gamma_2^t\right) = E\left(\Gamma_1^t\right) + E\left(\Gamma_2^t\right)$ is defined by (Chen et al., 2002):
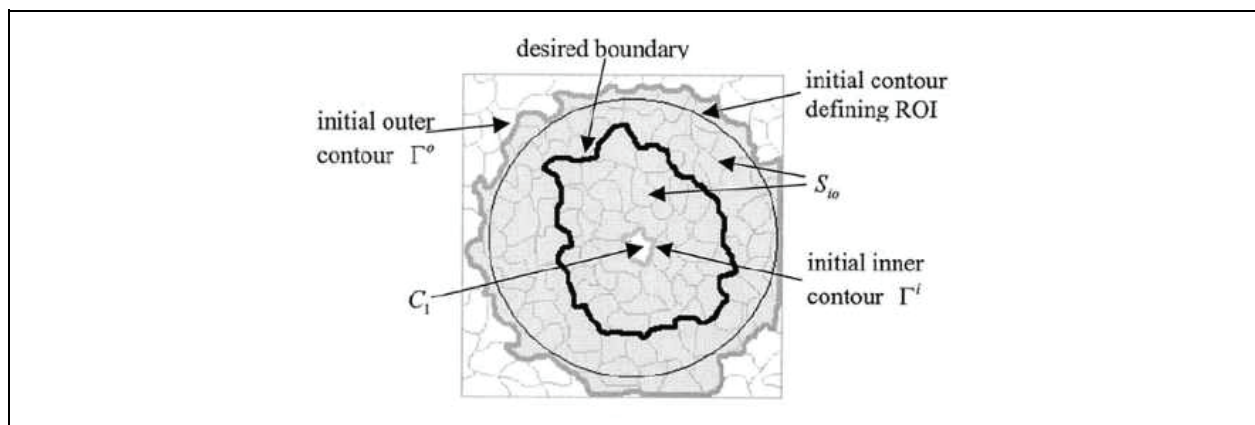
Fig. 5. Region of interest (ROI) and initial snakes. Reprinted from (Chen et al., 2002)

$$E\left(\Gamma_i^t\right) = \alpha_i E_{len}\left(\Gamma_i^t\right) + \beta_i E_\theta\left(\Gamma_i^t\right) + \gamma_i E_{ext}\left(\Gamma_i^t\right) + \delta_i E_{Area}\left(\Gamma_i^t\right). \tag{26}$$

where:

$$E_{len}\left(\Gamma_i^t\right) = \sum_{j=0}^{N-1} \left\| v_{i,j}^t - v_{i+1,j}^t \right\|, \tag{27}$$

$$E_\theta\left(\Gamma_i^t\right) = \sum_{j=0}^{N-1} \cos^{-1}\left(\frac{u_{i,j}^t - u_{i,j+3}^t}{\left\| u_{i,j}^t \right\| \left\| u_{i,j+3}^t \right\|}\right), \tag{28}$$

$$E_{ext}\left(\Gamma_i^t\right) = \sum_{j=0}^{N-1} \left\| \nabla I\left(v_{i,j}^t\right) \right\|, \tag{29}$$

$$E_{Area}\left(\Gamma_i^t\right) = Area\left(S_{io}^t\right), \tag{30}$$

where $v_{i,j}^t$ means the *jth* snaxel of the *ith* snake at time *t*, $u_{i,j}^t = v_{i,j}^t - v_{i,j-3}^t$, S_{io}^t denote the set of cells enclosed by the inner and outer snakes at the deformation step *t*, and $\alpha_i, \beta_i, \gamma_i, \delta_i$, $i = 0, 1, ..., N-1$ are real parameters that controls the influence of each term in the expression (26).

The first energy term E_{len} gives the perimeter of the contour Γ_j^t. If we take $\alpha_1 < 0$ and $\alpha_2 > 0$, then, minimizing this energy would force the inner snake into expanding outward and the outer snake into contracting. The term E_θ approximates the curvature along the snake and aims to control the smoothness of the contour.

The third energy E_{ext} is the external energy defined based on edge features. The last energy, E_{Area}, is the area covered by the cells in S_{io}^t. When minimizing energy (26) this term will provide the attraction force to pull the inner and the outer snakes to each other.

The energies (27)-(30) may have different ranges. Therefore, the target function to be minimized is the normalized energy variation $\Delta E\left(\Gamma_i^t\right)$ rather than the $E\left(\Gamma_i^t\right)$ itself, that is:

$$\Delta E\left(\Gamma_1^t, \Gamma_2^t; \Gamma_1^{t+1}, \Gamma_2^{t+1}\right) = \tag{31}$$

$$\alpha_i \Delta E_{len}\left(\Gamma_i^t\right) + \beta_i \Delta E_\theta\left(\Gamma_i^t\right) + \gamma_i \Delta E_{ext}\left(\Gamma_i^t\right) + \delta_i \Delta E_{Area}\left(\Gamma_i^t\right). \tag{32}$$

where $\Delta E_{len}\left(\Gamma_i^t\right), \Delta E_\theta\left(\Gamma_i^t\right), \Delta E_{ext}\left(\Gamma_i^t\right), \Delta E_{Area}\left(\Gamma_i^t\right)$ have the general form:

$$\Delta E\left(\Gamma_1^t, \Gamma_2^t; \Gamma_1^{t+1}, \Gamma_2^{t+1}\right) =$$

$$\frac{\left[E_\rho\left(\Gamma_1^{t+1}\right) + E_\rho\left(\Gamma_2^{t+1}\right)\right] - \left[E_\rho\left(\Gamma_1^t\right) + E_\rho\left(\Gamma_2^t\right)\right]}{\left[E_\rho\left(\Gamma_1^t\right) + E_\rho\left(\Gamma_2^t\right)\right]}$$

with $\rho \in \{len, \theta, ext, Area\}$ and $\alpha_i, \beta_i, \gamma_i, \delta_i$ are the same of expression (26).

Before to proceed, we need other definitions. Let S_1^t be the set of cells inside the ROI that intersect the curve Γ_1^t (similarly for S_2^t). Besides, it is defined in (Chen et al., 2002) the operators Φ and Ψ such that:

$$\Phi\left(S_{io}^t\right) = \Gamma_2^t \qquad and \qquad \Psi\left(S_{io}^t\right) = \Gamma_1^t. \tag{35}$$

The deformation of the model is based on the two operators called cell-erosion and the cell-dilation. These operators are described on Figure 6. The former, denoted by *CE*, is defined as:

$$CE\left(S_{io}^t, C_p\right) = S_{io}^t - \{C_p\}, \quad C_p \in \left(S_1^t \cup S_2^t\right) \cap S_{io}^t. \tag{36}$$

The cell-dilation, denoted by *CD*, is defined by:

$$CD\left(S_{io}^t, C_p\right) = S_{io}^t \cup \{C_p\}, \quad C_p \in \left(S_1^t \cup S_2^t\right) - S_{io}^t. \tag{37}$$

The cell-based dual snakes evolution is the greedy procedure that aims to minimize the normalized energy variation defined in expression (32). It is based on the following algorithm to find the minimum of the energy variation given by expression (32).
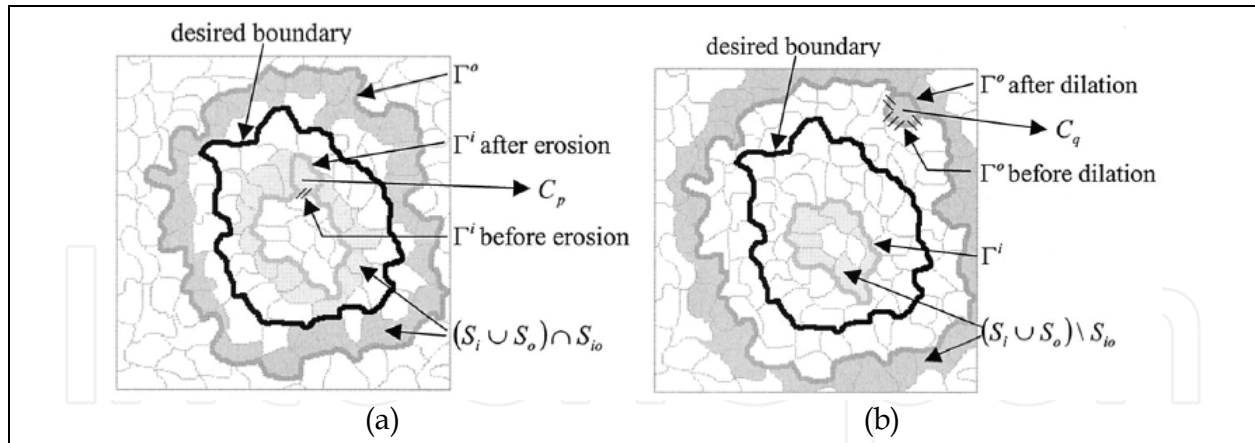
Fig. 6. (a)Erosion operator. (b) Dilation operation. Reprinted from (Chen et al., 2002)

1. Initialization: define S_{io}^0, $\Phi\left(S_{io}^0\right) = \Gamma_2^0$, $\Psi\left(S_{io}^0\right) = \Gamma_1^0$ and and set $t = 0$.

2. While $S_{io}^0 \neq \varnothing$,

$$C_e = \underset{C_p \in \left(S_1^t \cup S_2^t\right) \cap S_{io}^t}{\arg\min}\left\{\Delta E_{erode} = \Delta E\left(\Gamma_1^t, \Gamma_2^t; \Phi\left(CE\left(S_{io}^t, C_p\right)\right), \Psi\left(CE\left(S_{io}^t, C_p\right)\right)\right)\right\}, \quad (38)$$

$$C_d = \underset{C_p \in \left(S_1^t \cup S_2^t\right) - S_{io}^t}{\arg\min}\left\{\Delta E_{dilate} = \Delta E\left(\Gamma_1^t, \Gamma_2^t; \Phi\left(CD\left(S_{io}^t, C_p\right)\right) \cup \Psi\left(CD\left(S_{io}^t, C_p\right)\right)\right)\right\}, \quad (39)$$

2.1. If $\Delta E_{erode} < \Delta E_{dilate}$, $S_{io}^{t+1} = CE\left(S_{io}^t, C_e\right)$. Else, $S_{io}^{t+1} = CD\left(S_{io}^t, C_d\right)$.

2.2. $\Gamma_2^{t+1} = \Phi\left(S_{io}^{t+1}\right)$ and $\Gamma_1^{t+1} = \Psi\left(S_{io}^{t+1}\right)$.

Once the boundary is extracted based on this algorithm, some kind of smoothing process may be applied in order to improve it. This stage can be performed by an usual snake model, that is, the dual result is used to initialize a parametric (single) snake model. Other possibility, also discussed in (Chen et al., 2002), would be spline interpolation.

The Figure 7 pictures the stages of the method for breast ultrasound segmentation. Figure 7.a pictures the original image with a benign lesion. This input image is then filtered by a gaussian kernel followed by a Sobel edge detector. The cells generated by the watershed algorithm are pictured on Figure 7.b. The initialization of the method and the obtained result (white contour) are shown on Figures 7.c and 7.d, respectively.

4. Implicit models

In this section we review the implicit formulation for dual models: the Dual-Level-Set and the Dual-Front methods. The former maintains the philosophy of Dual-T-Snakes: one snake contracts and splits from outside the targets and another ones expand from inside the targets (section 3.2). However, the snake model will be the level set described on section 2.2. The later, the Dual-Front method, uses fast marching methods (Sethian, 1999) to propagate two action maps until they met each other generating an interface that represents the boundary. These action maps are derived from potentials that take lower values near the
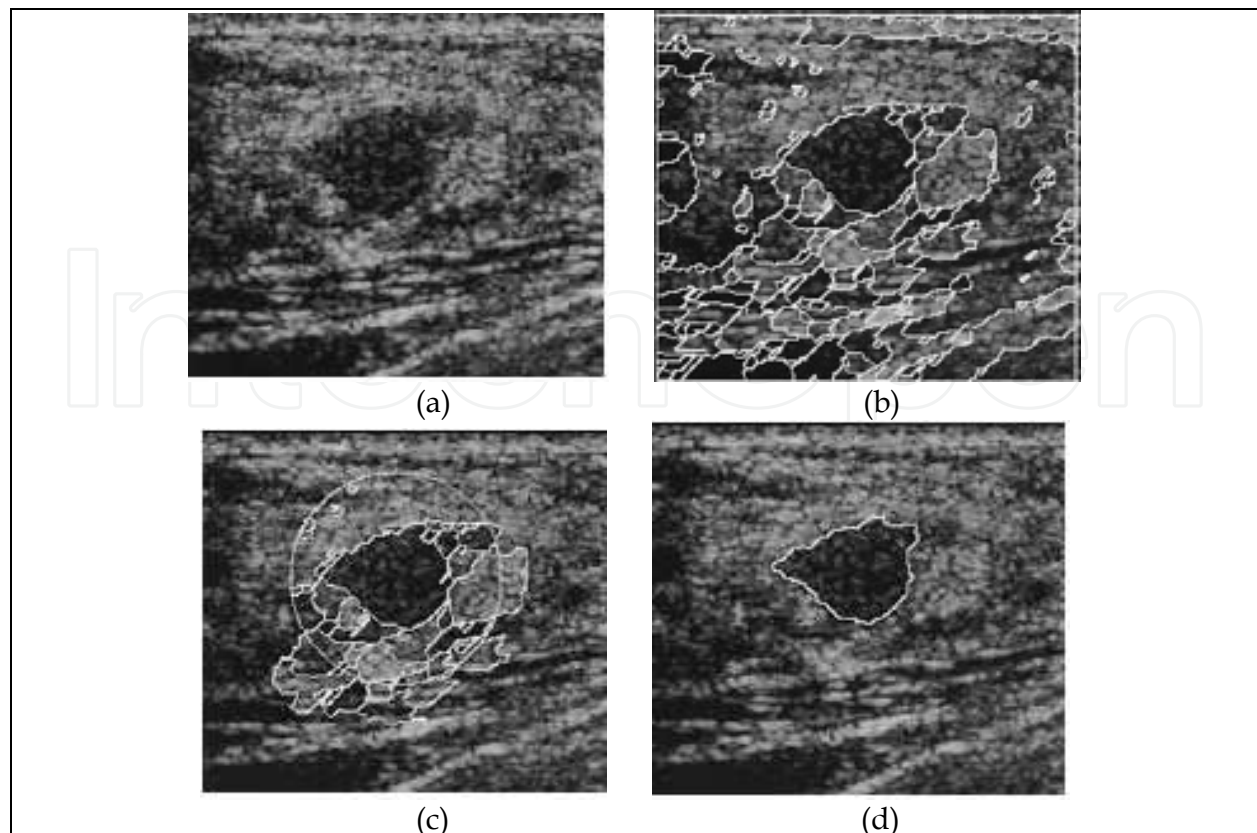
Fig. 7. (a)Original breast ultrasound image. (b) Cells generated by the watershed algorithm. (c)Initial snakes (white contours). (d) Final result. Reprinted from (Chen et al., 2002)

desired boundaries. So, both the Dual-Level-Set and the Dual-Front methods keep the idea of using two linked processes to seek for the global minimum.

4.1 Dual-Level-Set approach

In this section we maintain the philosophy of Dual-T-Snakes: one snake contracts and splits from outside the targets and another ones expand from inside the targets (section 3.2). However, the snake model will be an implicit one. To set ideas, let us consider the Figure 8.a, which shows two contours bounding the search space and Figure 8.b that pictures a surface which zero level set is the union of the two contours just presented.
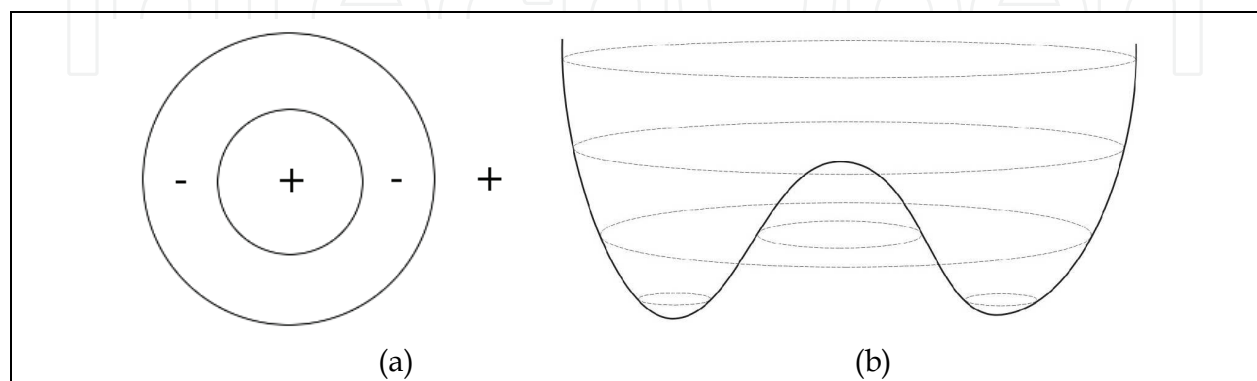
Fig. 8. (a)Dual snakes bounding the search space. (b) Initial function which zero level set is the two contours presented.

If the surface evolves such that the two contours get closer, we can obtain the same behavior of Dual-T-Snakes. That is the key idea of the method proposed by some of us in (Suri & Editors, 2006). In order to accomplish this goal we must define a suitable speed function and an efficient numerical approach. For simplicity, we consider the one dimensional version of the problem pictured on Figure 9. In this case, the level set equation given by expression (9) can be written as:

$$G_t + \frac{\partial G}{\partial x} F = 0. \tag{40}$$

The main point is to design the speed function F such that $G_t > 0$. Therefore, if we set the sign of F opposite to the one of G_x we get this goal, once:

$$G_t = -\frac{\partial G}{\partial x} F = 0. \tag{41}$$

Hence, the desired behavior can be obtained by the sign distribution of F, shown in Figure 9.
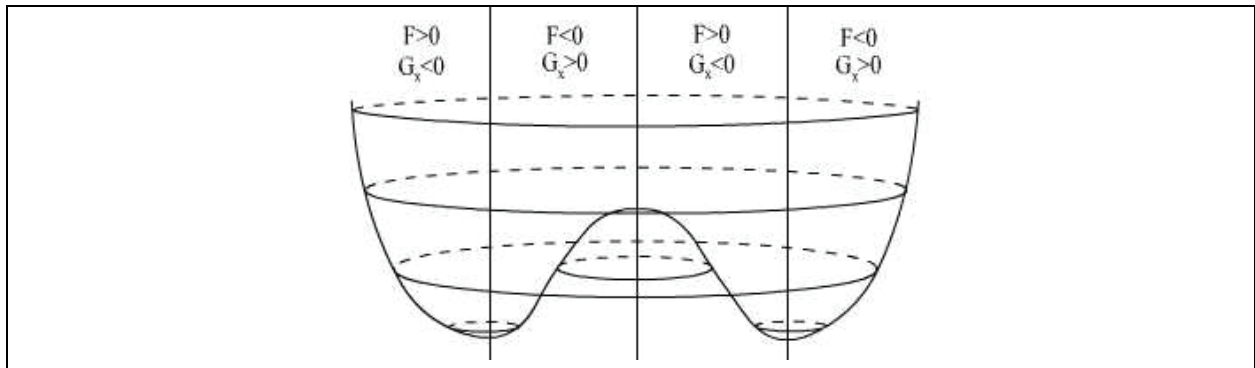
Fig. 9. Sign of speed function.

However, we should notice that $G_x = 0$ for singular points. So, the values of G remain constant over these points because G_t becomes null. Thus, we should be careful about the surface evolution nearby the singular points because anomalies may happen. One possibility to avoid this problem is to stop front evolution before getting close to this point. Another possibility could be to change the evolution equation in order to allow the $G_t \neq 0$ over singular points. Such proposal implies that the isolines may be not preserved, that is, they become a function of time also. Thus:

$$G(x(t), t) = y(t), \tag{42}$$

consequently, by applying Chain rule:

$$G_t + \frac{\partial G}{\partial x} \frac{dx}{dt} = \frac{dy}{dt}, \tag{43}$$

Therefore, we should provide an speed function in y direction.

$$G_t + \left(\frac{\partial G}{\partial x}, -1 \right) \cdot \left(\frac{dx}{dt}, \frac{dy}{dt} \right) = 0, \tag{43}$$

We can write this expression as:

$$G_t + F\|\nabla G, -1\| = 0, \tag{45}$$

where F is the speed function. For fronts in $3D$ we get:

$$G_t + \frac{\partial G}{\partial x}\frac{dx}{dt} + \frac{\partial G}{\partial y}\frac{dy}{dt} = \frac{dz}{dt}, \tag{46}$$

therefore:

$$G_t + \left(\frac{\partial G}{\partial x}, \frac{\partial G}{\partial y}, -1\right) \cdot \left(\frac{dx}{dt}, \frac{dy}{dt}, \frac{dz}{dt}\right) = 0, \tag{47}$$

One way to deal with these models is through viscous conservation laws (Sethian, 1996). For example, expression (43) becomes:

$$G_t + \frac{\partial G}{\partial x}\frac{dx}{dt} = \varepsilon \frac{\partial^2 G}{\partial x^2}, \tag{48}$$

If dy / dt is replaced by εG_{xx} where ε is a new parameter. For $2D$ we will have:

$$G_t + \left(\frac{\partial G}{\partial x}, \frac{\partial G}{\partial y}\right) \cdot \left(\frac{dx}{dt}, \frac{dy}{dt}\right) = \varepsilon \nabla^2 G, \tag{49}$$

where ∇^2 means the Laplace operator defined by:

$$\nabla^2 G = \frac{\partial^2 G}{\partial x^2} + \frac{\partial^2 G}{\partial y^2}. \tag{50}$$

In our model we will maintain the idea that the front evolves in the normal direction. Thus, expression (49) can be rewritten as:

$$G_t + F\|\nabla G\| = \varepsilon \nabla^2 G, \tag{51}$$

following the same development to derive expression (9). Such model has been studied in the context of front propagation in (Malladi et al., 1995; Sethian, 1996).

Once our application focus is shape recovery in a image I, we must choose a suitable speed function F as well as a convenient stopping term S to be added to the right-hand side of equation (51). Among the possibilities (Suri et al., 2002), the following ones have been suitable for our Dual-Level-Set:

$$F = \frac{1 + \alpha k}{1 + \|\nabla I\|^2}, \tag{52}$$

$$S = \beta \nabla P \cdot \nabla G, \tag{53}$$

where k is the curvature, defined by expression (11), α, β are scale parameters and $P = -\|\nabla I\|^2$. Therefore, we are going to deal with the following level set model:

$$G_t = \left(\frac{1 + \alpha k}{1 + \|\nabla I\|^2} \right) \|\nabla G\| + \varepsilon \nabla^2 G + \beta \nabla P \cdot \nabla G, \tag{54}$$

The evolution of the fronts follows this governing equation and are interdependent due to the embedding function. However, once the evolution stops, we must evaluate the similarity between the two contours and apply a driving velocity instead of the driving force of section 3.1. The numerical method is a first order one already known in the level set literature (Sethian, 1996). We have also simplified the initialization of the method through smoothed versions of step functions (see (Suri & Editors, 2006), for details).

As usual in level set approaches, we use the narrow band method; that is, only the values of G within a tube placed around the front are updated. When the front moves near to the edge of the tube boundary, the computation is stopped and a new tube is built with the zero level set at the center. For our dual approach, the narrow band is attractive not only for computational aspects but also because it allows an efficient way to evaluate similarity between two contours. In fact, instead of using the criterion of section 3.2, we take the procedure pictured on Figure 10: Firstly, the intersection point is computed (Figure 10.a); then, we take a neighborhood of this point (Figure 10.b) and stop to update the function G in all the grid points inside it or we can set to zero the speed function for these points. We say that those grid points are frozen ones.


(a)   (b)
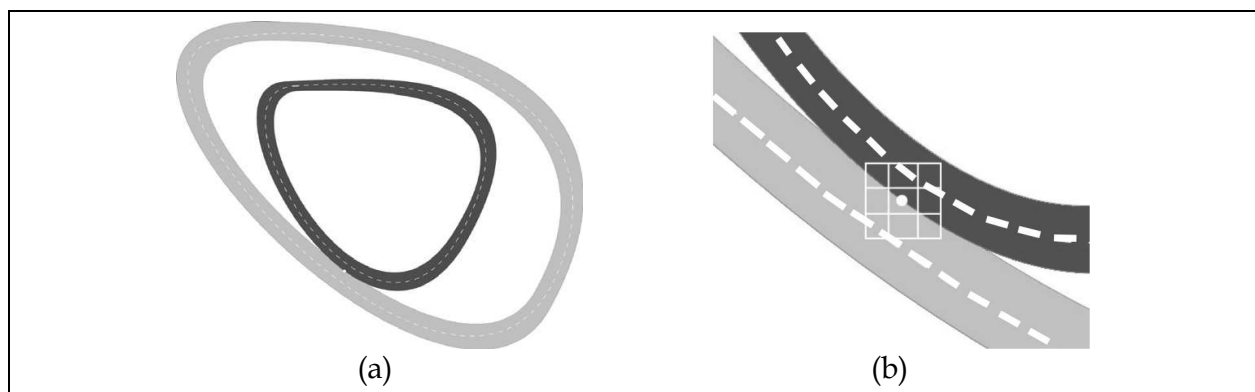
Fig. 10. (a)Narrow bands touching each other. (b) Neighborhood to define similarity between fronts.

Once the fronts stop moving, we must decide in which grid points we add a driving velocity. It is an extra velocity term which goal is the same of the driving force in section 3.2; that is, to keep fronts moving again. Therefore, we get a less sensitive model to the initial position of the fronts. To accomplish this task we can add an extra velocity term to equation (54), called V_{drive}.

We must be careful when choosing the grid points to apply this term. As in the case of Dual-T-Snakes, the fronts may be nearby the boundary somewhere, but far away from the target in another place. We should automatically realize this fact when the fronts stop moving. To accomplish this, we can use the affinity operator explained on section 3.2. Based on this operator, we can define an affinity function that assigns to a grid point inside the narrow band a $0-1$ value: 0 for the grid points most likely to lie away from the target boundaries and 1 otherwise. Like in the Dual-T-Snakes, such affinity operator can be defined through fuzzy segmentation methods (Giraldi et al., 2003), image transforms (Falcão et al., 2001),

region statistics, etc. The whole Dual-Level-Set algorithm can be summarized as follows: (1) Initialization through Step Functions; (2) Evolution until fronts stop. (3) Evaluate similarity. If frozen, stop. (4) Add V_{drive} for some time steps. (5) After that, turn-off V_{drive}. Go to step 2.

Likewise in the Dual-T-Snakes model, when all the grid points inside the narrow bands are frozen, we stop the Dual-Level-Set evolution and apply a search based algorithm to get the final result.

Figure 11 shows the application of the Dual-Level-Set to segment the cell image of Figure 11.a. However, instead of taking a band-pass version of it, like in Figure 4.b, we just apply a low pass filter to smooth the image. The Dual-Level-Set parameters are: $\alpha = 0.1$, $\varepsilon = 2.0$, $\beta = 0.1$, $T = 150$, $\Delta t = 0.05$.
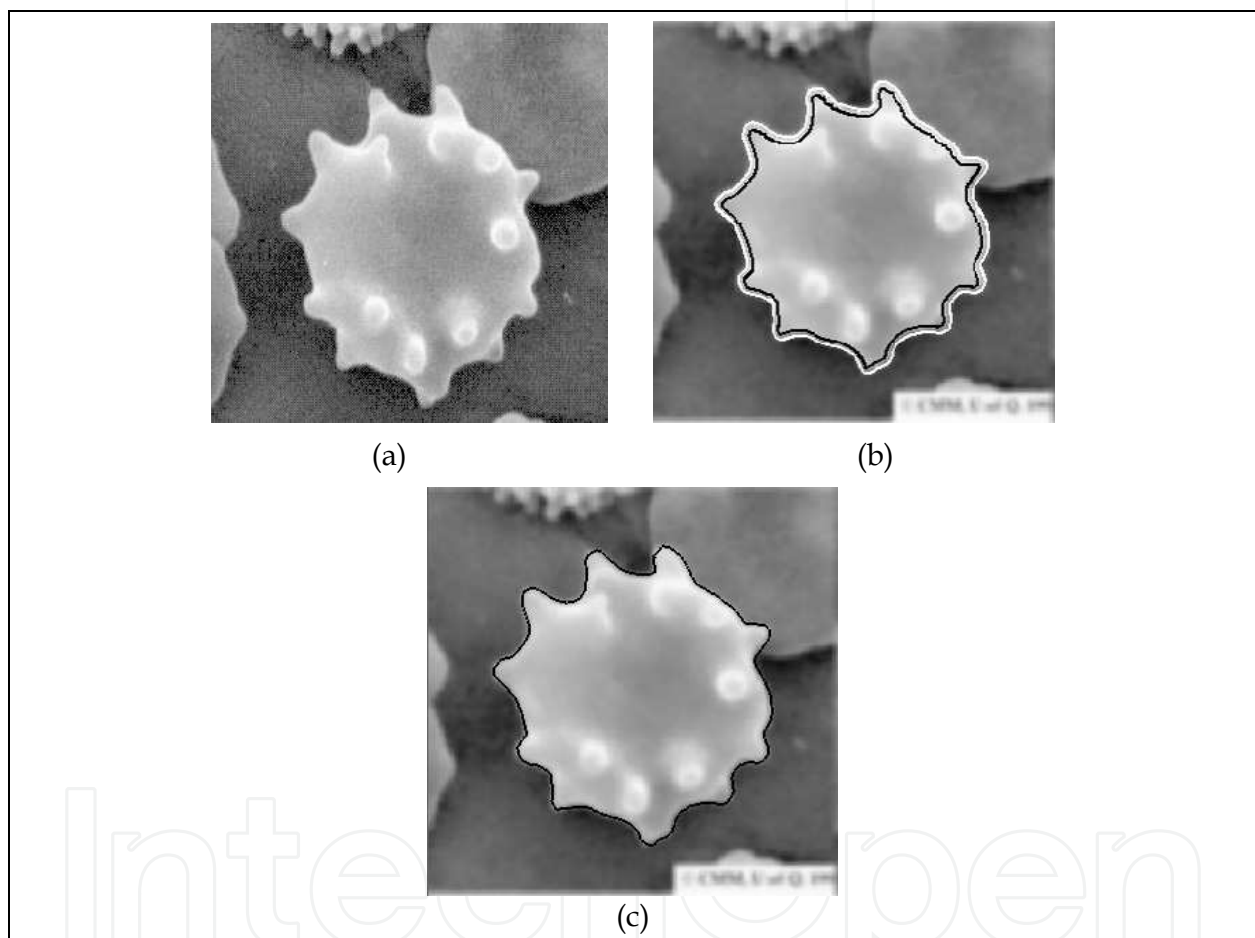
Fig. 11. (a) Original image. (b) Dual-Level-Set result. (c) Final result.

Once the two snakes in Figure 3 are very close to each other, a search method based on a greedy algorithm can be efficient and less expensive then the Viterbi (section 3.2). Firstly, we compute a curve located in-between the two fronts by taking the midpoint of each segment of the search space in Figure 3. The obtained curve can be used to initialize a snake model based on a greedy algorithm that works as follows (Suri & Editors, 2006). For each snaxel v_i we take a 3×3 neighborhood V, and for each pixel $p \in V$ we compute:

$$E(p) = \alpha E_{\text{int}}(v_{i-1}, p, v_{i+1}) + \beta E_{ext}(p) + \lambda E_{line}(p). \tag{55}$$

where E_{int}, E_{ext} and E_{line} are defined in equations (24) and (25), respectively. Then, we solve the problem:

$$p_0 = \arg\min\{E(p); \quad p \in V\}.$$ (56)

If $E(p_0) < E(v_i)$ then $v_i \leftarrow p_0$. The Figure 11.c pictures the obtained result.

4.2 Dual-Front approach

In (Li & Yezzi, 2005), a fast and flexible dual-front implementation of active contours is proposed by iteratively dilating an initial curve to form a narrow region and then finding the new closest potential weighted minimal partition curve inside. The method is motivated by minimal path technique (Cohen & Kimmel, 1996; Cohen, 2001). In this method, given a potential $P > 0$ and a point p in the domain Ω, the minimal action map $U_0(p)$ is defined as:

$$U_0(p) = \min_{A_{p_0,p}} \int_\Omega \overline{P}(c(s)) ds,$$ (57)

where $\overline{P} = P + w$, with w been a constant, and $A_{p_0,p}$ is the set of paths connecting p_0 and p. Expression (57) gives the minimal energy integrated along the paths between the starting point p_0 and any point p inside the domain Ω. Because the action map U_0 has only one minimum value at the starting point p_0 and is a convex function in Ω, it can be easily determined by solving the equation (Cohen & Kimmel, 1996):

$$\|\nabla U_0\| = \tilde{P}, \quad and \quad U_0 = 0.$$ (58)

If we set $\tilde{P} = 1/V$ then this expression becomes the so called Eikonal equation which can be efficiently solved by using fast marching methods (Sethian, 1999). Equations (57)-(58) are the starting point for the dual-front technique (Li & Yezzi, 2005). So, given two points $p_0, p_1 \in \Omega$, the method computes the action maps $U_0(p)$ and $U_1(p)$, respectively, through the solution of expression (58), seeking for the points $p \in \Omega$ such that:

$$U_0(p) = U_1(p).$$ (59)

At these points, the level set of the minimal action map U_0 meets the level set of the minimal action map U_1 generating the Voronoi diagram that decomposes the whole image into two regions containing the points p_0 and p_1. We can generalize definition (57) for a set $X \subset \Omega$ through the expression:

$$U_X(q) = \min_{p \in X} U_p(q),$$ (60)

that mens, $U_X(q)$ is the minimal energy along the paths of the set $A_{p,q}$ where $p \in X$. Therefore, given two curves c_{in} and c_{out} bounding the search space called R_n in the Figure 12, and two potentials $\tilde{P}_{in}$ and $\tilde{P}_{out}$ that takes lower values near desired boundaries, the dual-front algorithm firstly computes the minimal action maps U_{in} and U_{out} until these two

action maps meet each other. Then, the evolutions of the level sets of both the action maps stops and a minimal partition boundary is formed in the region R_n of the Figure 12. Mathematically, this boundary is the solution of the following equations:

$$\|\nabla U_{in}\| = \tilde{P}_{in}, \quad with \quad U_{in}(c_{in}) = 0, \tag{61}$$

$$\|\nabla U_{out}\| = \tilde{P}_{out}, \quad with \quad U_{out}(c_{out}) = 0, \tag{62}$$

$$U_{in}(p) = U_{out}(p). \tag{63}$$
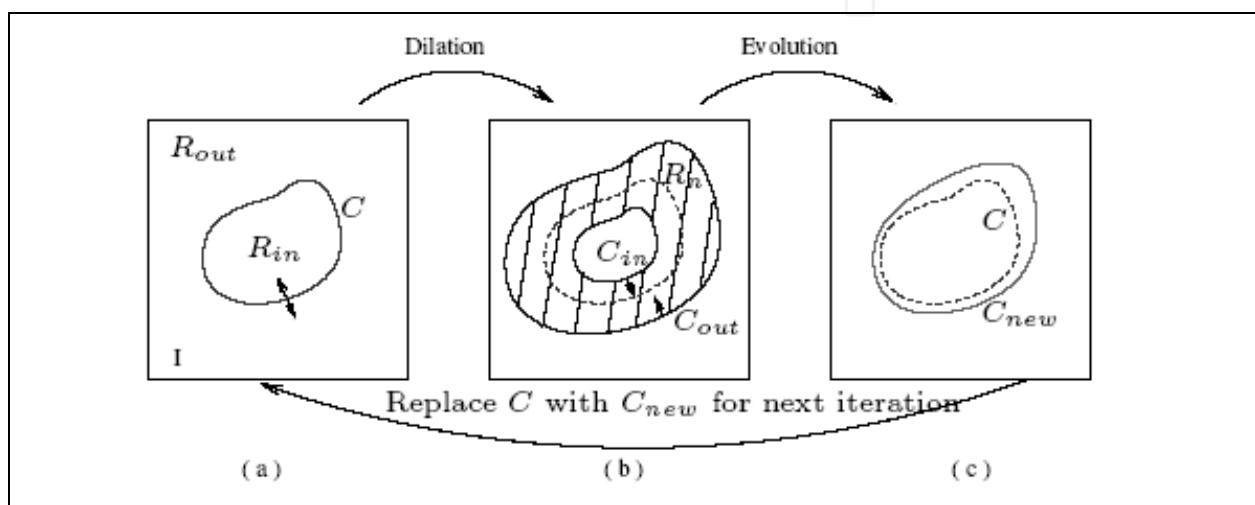
Fig. 12. One interaction of the Dual-Front algorithm. (a) Initial curve $C = c_n$ of the iteration n. (b) Search space defined through dilation of the initial curve c_n with bounds c_{in} and c_{out}. (c) Obtained solution C_{new}, the minimal partition curve. The curve C is replaced by the curve C_{new} to initialize the next iteration. Reprinted from (Li & Yezzi, 2005)

The dual-front approach is an iterative method which is picture on Figure 12. Firstly, the curves c_{in} and c_{out} are placed by user interaction or obtained by dilation of an initial curve, named by C in Figure 12. Then, the minimal partition boundary is computed by solving equations (61)-(63). To perform this task, the actions U_{in} and U_{out} are computed inside the region R_n, through expressions (61) and (62), respectively, until condition (63) is achieved. The obtained result, named by c_{n+1} will replace C for processing the next iteration. The method proceed until the distance between consecutive minimal partition curves is less than a pre-defined threshold δ, that means $d(c_n, c_{n+1}) < \delta$ (like in expressions (19)). The potentials $\tilde{P}_{in}$ and $\tilde{P}_{out}$ are defined in (Li & Yezzi, 2005) using the following general expressions which integrates region based and the edge-based information.

$$\tilde{P}_{in} = w_{in}^r \cdot f\left(\left|I(x,y) - \mu_{in}\right|, \sigma_{in}^2\right) + w_{in}^b \cdot g(\nabla I) + w_{in}, \tag{64}$$

$$\tilde{P}_{out} = w_{out}^r \cdot f\left(\left|I(x,y) - \mu_{out}\right|, \sigma_{out}^2\right) + w_{out}^b \cdot g(\nabla I) + w_{out}, \tag{65}$$

where μ_{in}, σ_{in}^2 are the mean and variance of the image intensity inside region $(R_{in} - R_{in} \cap R_n)$, $\mu_{out}, \sigma_{out}^2$ are the mean and variance of the image intensity inside region $(R_{out} - R_{out} \cap R_{in})$, and $w_{in}^r, w_{in}^b, w_{in}$ are parameters to be set in advance (the same for $w_{out}^r, w_{out}^b, w_{out}$).

The Figure 13 shows an example of the application of the dual-front method for 2D human brain MRI image where the segmentation objective is to find the interface between the gray matter and the white matter. This example is interesting to observe the sensitivity of the method against the width of the search space, called active region in (Li & Yezzi, 2005). We observe that the obtained result was much better for the narrower search space than for the other ones. In this test, the potentials in expressions (64)-(65) are defined by setting $w_{in}^r = w_{out}^r = 1$, $w_{in}^b = w_{out}^b = 0.1$, $w_{in} = w_{out} = 0.1$, and f, g given by:

$$f(x,y) = |I(x,y) - \mu_{in}|, \qquad (66)$$

$$g(x,y) = |1 + (\nabla I)^2|, \qquad (67)$$
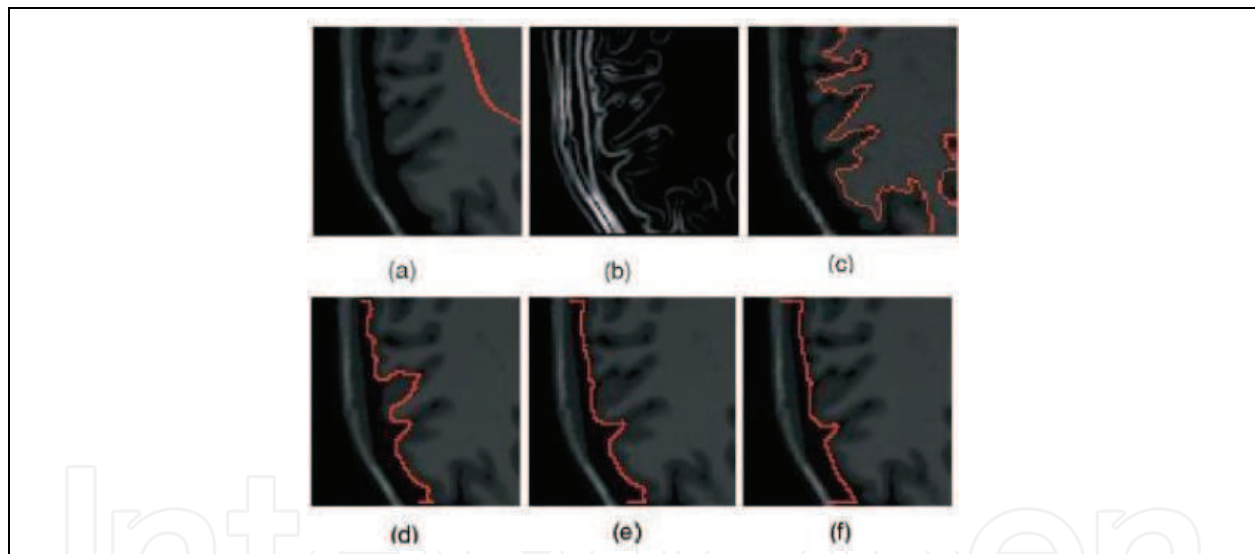
Fig. 13. Sensitivity of the of the Dual-Front against different sizes of the active region (search space): (a) The original *2D* human brain MRI image and the initial curve; (b) The corresponding edge map obtained through the gradient information; (c)-(f) Segmentation results obtained for a search space defined through morphological dilation of the initial curve with 5×5, 7×7, 11×11, 15×15 pixels circle structuring elements, after 15 iterations, respectively. Reprinted from (Li & Yezzi, 2005)

5. Discussion

An important point for dual snakes is how to proceed the evolution after both snakes comes at rest but are far from each other. The affinity operator in the Dual-T-Snakes and Dual-Level-Set models is used in this step, in order to avoid that some snaxels pass over the

desired boundary, due to the driving term. Such procedure is bypassed in the original dual model (section 3.1) due to the shape model used. The corresponding energy term may prevents that a snake pass over a global minimum. However, the shape model given by expression (12) limits the application of the method for general shapes and topologies.

On the other hand, in the cell-based dual model, the cell decomposition of the image domain provided by the watershed strongly reduces the search space. Therefore, the energy minimization method may be less sensitive to local minima. That is way authors do not take care about the possibility of snakes reach equilibrium position far from the target. However, it does not seems to be possible to prove that such situation never happens.

In the Dual-Front, actually the level sets of the action map U give the evolution of the front. The velocity of the evolving front is decided by the potential. Therefore, both the potentials in expressions (64)-(65) must be defined such that the velocity is much lower when the evolving fronts arrive the boundary. If the constant $w > 0$, the front velocity will be never null, and so, fronts only stop when the two action maps meet each other. Such policy is interesting to pass over local minima but once there is no an energy balance between fronts the global minimum may be also lost.

Dual-Level-Set as well as Dual-T-Snakes are topologically adaptable deformable models which increases their range of applications. However, such generality has also a price: the care with local minima should be higher than in the original model, for example, because there is no a shape model to bias the solution to the desired shape.

Also, the characteristic function in the Dual-T-Snakes plays a similar role of the embedding function for the Dual-Level-Set in the sense that they provide the framework for topological changes. However, the update of the former is based on exhaustive tests (McInerney & Terzopoulos, 1999) while the later is just a consequence of the model evolution based on the equation (54). As a practical consequence, we observed that it is easier to implement the Dual-Level-Set than the Dual-T-Snakes. Also, we observe in our experiments that sometimes it is more efficient to apply topologically adaptable dual models just to reduce the search space, and, then to apply a search based technique to get the final result. This procedure was exemplified in sections 3.2 and 4.1. It is attractive because it simplifies the choice of parameters for the dual method and makes the computational cost of the application of a global optimization technique smaller.

Despite of the capabilities to reject local minima, dual models have also some disadvantages. Firstly, the method is at least two times more expensive than single approaches. Secondly, the initialization may be a tedious task because the user should set two curves at the beginning of the process. The choice of parameter values is also another point to be careful because in this case there are two snakes to be set.

A fundamental and more difficult point for dual snakes is how to proceed the evolution after both snakes comes at rest but they are far from each other. The snake with higher energy must be evolved, but the method should automatically realize the snaxels most likely to lie away from the boundary. The affinity operator (section 3.2) was proposals to address this problem without imposing restrictions to the snake evolution.

6. Conclusions and the future of dual methods

The original dual approach is an interesting technique to address the sensitivity to local minima of usual snake models. The idea of using two snakes to seek for the global minimum, originally proposed in (Gunn & Nixon, 1997), have been used and extended in

recent works. Topological capabilities were incorporated, implicity formulations were developed and a cell-based approach were designed in order to improve the efficiency. This chapter offered a review of these state-of-the-art techniques as well as the background behind dual approaches.

Dual methods can avoid local minima through the comparison between the two contours energy and positions but they are at least two times more expensive than single approaches. Therefore, the ultrasound images seems to be the main target for the application of dual snakes because the difficulties inherent to the segmentation of these images force the application of a more robust approach against local minima.

The application of GPU techniques (Lefohn et al., 2003) must be considered in further works in order to improve the performance of the dual methods. The development of *3D* dual approaches is another point. For example, Dual-Level-Set as well as Dual-T-Snakes can be easily extended to *3D* without any extra machinery. Both the Dual-T-Snakes and the Dual-Level-Set methods are suitable for a parallel implementation in shared memory machines because, in the implicit formulation we must distribute the narrow band evolution while in the parametric case we should focus in the distribution of the T-Snakes processing. Multigrid techniques can be also implemented in both methods through Adaptive Mesh Refinement schemes (Giraldi et al., 2000a; Sethian, 1996).

7. Acknowledgment

8. References

Amini, A. A., Weymouth, T. E. & Jain, R. C. (1990). Using dynamic programming for solving variational problems in vision, IEEE Trans. on Pattern Analysis and Machine Intel. 12(9): 855–867.

Bamford, P. & Lovell, B. (1997). A two-stage scene segmentation scheme for the automatic collection of cervical cell images, Proceedings of TENCON '97, Brisbane, Australia. Bischoff, S. & Kobbeit, L. (2004). Snakes with topology control, The Visual Computer 20: 217–228.

Chen, C.-M., LU, H. H.-S. & HSIAO, A.-T. (2001). A dual-snake model of high penetrability for ultrasound image boundary extraction, Ultrasound in Med. Biol. 27(12): 16511665.

Chen, C.-M., LU, H. H.-S. & HUANG, Y.-S. (2002). Cell-based dual snake model: A new approach to extracting highly winding boundaries in the ultrasound images, Ultrasound in Med. Biol. 28(8): 10611073.

Cohen, L. (2001). Multiple contour finding and perceptual grouping using minimal paths, Journal of Mathematical Imaging and Vision 14: 225–236.

Cohen, L. D. (1991). On active contour models and balloons, CVGIP:Image Understanding 53(2): 211–218.

Cohen, L. & Kimmel, R. (1996). Global minimum for active contour models: A minimal path approach, IEEE International Conference on CVPR (CVPR'96), pp. 666–673. Davatzikos, C. & Prince, J. (1999). Convexity analysis of active contour algorithms, Image and Vision Computing 17(1): 27–36.

Falco, A., da Cunha, B. & Lotufo, R. (2001). Design of connected operators using the image foresting transform, SPIE on Medical Imaging, Vol. 4322, pp. 468–479.

Giraldi, G. A. & Oliveira, A. A. F. (2004). Invariant snakes and initialization of deformable models, Int. J. Image Graphics 4(3): 363–384.

Giraldi, G. A., Strauss, E. & Oliveira, A. F. (2000a). A boundary extraction approach based on multi-resolution methods and the T-snakes framework, International Symposium on Computer Graphics, Image Processing and Vision (SIBGRAPI'2000).

Giraldi, G. A., Strauss, E. & Oliveira, A. F. (2000b). A boundary extraction method based on Dual-T-Snakes and dynamic programming, IEEE Computer Society Conference on Computer Vision and Pattern Recognition (CVPR'2000).

Giraldi, G. A., Strauss, E. & Oliveira, A. F. (2003). Dual-T-Snakes model for medical imaging segmentation, Pattern Recognition Letters 24(7): 993–1003.

Gunn, S. R. (1996). Dual Active Contour Models for Image Feature Extraction, PhD thesis, Faculty of Engineering and Applied Science, Department of Eletronics and Computer Science.

Gunn, S. R. & Nixon, M. S. (1997). A robust snake implementation; a dual active contour, IEEE Trans. Pattern Anal. Mach. Intell 19(1): 63–68.

Ip, H. H. S. & Shen, D. (1998). An affine-invariant active contour model (ai-snake) for modelbased segmentation, Image and Vision Computing 16(2): 135–146.

Kass, M., Witkin, A. & Terzopoulos, D. (1988). Snakes: Active contour models, International Journal of Computer Vision 1(4): 321–331.

Lefohn, A., Cates, J. E. & Whitaker, R. T. (2003). Interactive, gpu-based level sets for 3d segmentation, In: Medical Image Computing and Computer Assisted Intervention (MICCAI), pp. 564–572.

Leymarie, F. & Levine, M. D. (1993). Tracking deformable objects in the plane using and active contour model, IEEE Trans. Pattern Anal. Mach. Intell. 15(6): 617–634.

Li, H. & Yezzi, A. (2005). Local or global minima: flexible dual front active contours, Proc. Of Workshop-Comp. Vis. for Biom. Image App. (CVBIA 05, pp. 356–366.

Malladi, R., Sethian, J. A. & Vemuri, B. C. (1995). Shape modeling with front propagation: A level set approach, IEEE Trans. Pattern Anal. Mach. Intell. 17(2): 158–175.

McInerney, T. & Terzopoulos, D. (1996). Deformable models in medical image analysis: A survey, Medical Image Analysis 1(2).

McInerney, T. & Terzopoulos, D. (1999). Topology adaptive deformable surfaces for medical image volume segmentation, IEEE Trans. on Medical Imaging 18(10): 840–850.

Oliveira, A., Ribeiro, S., Farias, R., Esperanca, C. & Giraldi, G. (2004). Loop snakes: Snakes with enhanced topology control, SIBGRAPI '04, pp. 364–371.

Sapiro, G. (1997). Color snakes, Computer Vision and Image Understanding 68(2): 247–253.

Sethian, J. A. (1996). Level Set Methods: Evolving Interfaces in Geometry, Fluid Mechanics, Computer Vision and Materials Sciences, Cambridge University Press.

Sethian, J. A. (1999). Fast marching methods, SIAM Review 41: 199–235.

Suri, J. & (Editors), A. F. (eds) (2006). deformable models: clinical and biological applications, Springer, NY.
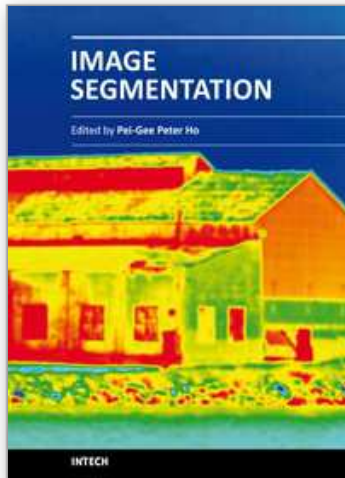
It was estimated that 80% of the information received by human is visual. Image processing is evolving fast and continually. During the past 10 years, there has been a significant research increase in image segmentation. To study a specific object in an image, its boundary can be highlighted by an image segmentation procedure. The objective of the image segmentation is to simplify the representation of pictures into meaningful information by partitioning into image regions. Image segmentation is a technique to locate certain objects or boundaries within an image. There are many algorithms and techniques have been developed to solve image segmentation problems, the research topics in this book such as level set, active contour, AR time series image modeling, Support Vector Machines, Pixon based image segmentations, region similarity metric based technique, statistical ANN and JSEG algorithm were written in details. This book brings together many different aspects of the current research on several fields associated to digital image segmentation. Four parts allowed gathering the 27 chapters around the following topics: Survey of Image Segmentation Algorithms, Image Segmentation methods, Image Segmentation Applications and Hardware Implementation. The readers will find the contents in this book enjoyable and get many helpful ideas and overviews on their own study.

INTECH

open science | open minds